Journal of Sound and Vibration 555 (2023) 117703

Contents lists available at ScienceDirect

Journal of Sound and Vibration

journal homepage: www.elsevier.com/locate/jsvi

Viscoelastic damping design – A novel approach for shape optimization of Constrained Layer Damping treatments at different ambient temperatures

Martin Gröhlich [a,b,*], Marc Böswald [a,b], Jörg Wallaschek [c]

[a] German Aerospace Center (DLR), Institute of Aeroelasticity, Bunsenstraße 10, 37073 Göttingen, Germany
[b] Cluster of Excellence SE^{2}A – Sustainable and Energy-Efficient Aviation, Technical University Braunschweig, Germany
[c] Leibniz University Hannover, Institute of Dynamics and Vibration Research (IDS), An der Universität 1, 30823 Garbsen, Germany

ARTICLE INFO

Keywords:
Constrained Layer Damping
Viscoelastic damping design
Geometric shape optimization

ABSTRACT

Passive damping plays an important role in the vibration mitigation of aeronautic structures. In contrast to active systems, passive damping systems do not require any energy supply. Thus, their readiness is independent, which reduces the failure probability compared to active systems. Constrained Layer Damping (CLD) has become an established treatment for damping bending vibrations. Unlike other passive systems such as shock-mounts, CLD can be compactly integrated into an existing structure as an add-on solution. However, the design scope is limited by mass constraints and the optimal design for maximum damping must be found by optimization. For this purpose, a novel optimization approach is presented. The layer widths of the core and face layers of a CLD structure are treated as design parameters. Compared to the strategy of placing CLD patches on vibration antinodes, the proposed approach provides up to 52 % higher damping. The optimal design of a generic beam structure is determined considering different modes, viscoelastic material stiffnesses and ambient temperatures. Furthermore, the simulated damping is experimentally verified for a shape-optimized beam. The analyses show that the optimal design depends significantly on the viscoelastic material stiffness and is therefore temperature dependent. As a consequence, a generalized design guideline for CLD treatments cannot be derived.

1. Introduction

Passive vibration damping plays a key role in the design of lightweight structures, especially in aeronautics and in the design of aircraft components [1,2]. An advantage over active systems is that passive systems do not require a proof of failure probability or a wired connection to an energy source, which usually results in an unwanted mass gain. The aircraft design process is dominated by stringent aeroelastic and fatigue requirements. Vibrations caused by gusts or flight maneuver can impair the controllability of an aircraft and define the sizing loads for the design process. Moreover, vibrations arising from operating engines or from the turbulent boundary layer are transmitted to the fuselage as structure-borne sound. The resulting sound radiation from the fuselage skin contributes to the noise and further reduces the acoustic comfort of the passengers. Reducing structural vibration by integrated damping mechanisms would therefore be beneficial for load alleviation and a silent cabin. However, damping is usually not considered in the

* Corresponding author.
E-mail address: Martin.Groehlich@dlr.de (M. Gröhlich).

https://doi.org/10.1016/j.jsv.2023.117703
Received 12 September 2022; Received in revised form 9 March 2023; Accepted 4 April 2023
Available online 5 April 2023
0022-460X/

initial design phase of aeronautic structures.

The integration of passive damping mechanisms can be realized by using viscoelastic materials. Due to their chemical composition, such materials exhibit a high damping capacity. This characteristic makes viscoelastic materials attractive for structural vibration damping in engineering applications [1]. The mechanical properties of viscoelastic materials are highly frequency- and temperature-dependent [2–8]. However, this dependence can be described mathematically by appropriate models. The most prominent examples to represent the frequency dependence are the Generalized Maxwell-Modell (GMM) [7], the Golla-Hughes-McTavish-Modell [9], the model of fractional derivatives [10] and the Anelastic Displacement Fields model [11]. Additionally, the temperature dependence is typically modelled by the Williams-Landel-Ferry (WLF) equation [5]. A comprehensive review of research on these topics is given in [12,13].

An efficient way to incorporate viscoelastic materials for damping of flexural vibration was originally proposed by Kerwin [14]. Kerwin analyzed a three-layer composite structure with a compliant viscoelastic core. This configuration, known as Constrained Layer Damping (CLD), provides considerable damping, due to forced shear strain in the viscoelastic layer. Several analytical CLD models have been developed to determine the fundamental dynamic behavior under various boundary conditions [15–18]. With the increasing application of the finite element method (FEM), the appropriate FE modelling of CLD treatments became highly relevant and has been studied in particular by Moreira et al. and Araújo et al. [19–23]. Nowadays, the current research still deals with the analytical modelling of CLD treatments with an emphasis on complex structures and smart materials. Recent work includes the integration of material and geometric nonlinearities, magnetorheological elastomers and strain-dependent effects, as proposed by Li et al. [24–27].

The availability of analytical and numerical modelling approaches has motivated several authors to increase the damping efficiency of CLD treatments within an optimization framework. In this context, various geometrical or material-related quantities have been considered as design variables with additional constraints regarding mass gain or mechanical properties. The spectrum of design variables encompasses

- the thicknesses of core and face layer [28],
- the position and length of CLD patches [29,30],
- the position and shape of a CLD treatment [31],
- the cut position for segmenting fully covered CLD treatments [32],
- the elastic ply orientation angles and thicknesses of different laminated layers [33] and
- the amount and the material type of laminated layers [34].

A special class of structural optimization is the topology optimization [35]. In topology optimization, each finite element acts as a design variable and its material contribution to the mechanical system is determined based on calculated sensitivities. A pattern of elements is obtained that corresponds to the optimal design for achieving a maximum or minimum objective value. This technique has been applied to viscoelastic damping design in the last decade [36–39]. Latest advances encompass the work of Zhang et al. who introduced a hierarchical optimization algorithm for minimizing the sound power radiation of plates with CLD material [40]. Moreover, Fotsing et al. proposed a generalized rule of thumb for placing damping material at the antinodes of a mode shape [41]. Other studies have focused on placing damping treatment at locations with the highest modal strain energy [37,42,43].

However, a review of the state of the art reveals some knowledge gaps which are addressed in this paper:

I. One design parameter that has not been previously considered for damping optimization of CLD treatments, is the width of the core and face layers. Gröhlich et al. [44] showed that the damping of CLD beams is significantly affected by different widths of the layers. This approach is adopted here and formulated as an optimization problem with multiple widths.
II. It is well known that temperature has a significant impact on the mechanical properties of viscoelastic materials. However, the influence of temperature on the optimal design of CLD treatments has not yet been considered in damping optimization. Therefore, by applying the proposed optimization approach together with a fully characterized viscoelastic material, it is analyzed whether the optimal design of a CLD treatment is temperature-dependent.

The content of the paper is organized as follows: Chapter 1 provides an introduction and literature review of CLD treatments. The fundamentals of frequency- and temperature-dependent viscoelastic material modeling and corresponding analysis methods are exemplified in Chapter 2. Chapter 3 presents the new approach for shape optimization of CLD beams regarding maximum damping. The basic structure of the algorithm is introduced and the application is demonstrated by an example with two design variables. In Chapter 4, the optimization approach is analyzed with respect to the trade-off between numerical cost and accuracy of the results and compared to common placement strategies from the literature. Chapter 5 covers the application of the optimization approach to a CLD beam with a core layer consisting of a fully characterized bromobutyl rubber blend. The influence of temperature on the optimal design is analyzed and the result of a shape-optimized structure is experimentally validated. In Chapter 6, the key points of this paper are summarized and the main conclusions are drawn.

2. Theoretical background of viscoelastic damping

In this section, the fundamentals of viscoelastic damping are briefly discussed. The basic equations for modeling the frequency and temperature dependence are presented. Subsequently, an appropriate analysis method to evaluate systems with frequency-dependent properties is explained.

2.1. Viscoelastic material modeling

Viscoelastic materials exhibit frequency and temperature-dependent behavior. Considering harmonic steady-state excitation, the linear viscoelastic properties can be expressed in terms of a complex modulus E^*

$$E^*(\omega, T) = E^{'}(\omega, T) + \mathrm{i}E''(\omega, T), \tag{1}$$

where ω is the angular frequency, T the temperature and i the imaginary unit. The elastic part is indicated by the storage modulus $E^{'}$, while the loss modulus E'' describes the dissipative part. The key parameter for assessing the damping capability of a linear viscoelastic material is the ratio of the loss and storage moduli, denoted as material loss factor $\tan(\delta)$

$$\tan(\delta(\omega, T)) = \frac{E''(\omega, T)}{E^{'}(\omega, T)}. \tag{2}$$

In this paper, the GMM is used to model the frequency dependence. In this case, the storage and loss moduli are defined as a Prony series consisting of several relaxation times τ_i and elastic moduli E_i obtained from curve fitting of measured data

$$E^{'}(\omega) = E_\infty + \sum_{i=1}^{n} E_i \frac{\omega^2\tau_i^2}{1+\omega^2\tau_i^2}, \tag{3}$$

$$E''(\omega) = \sum_{i=1}^{n} E_i \frac{\omega\tau_i}{1+\omega^2\tau_i^2}. \tag{4}$$

In eq. (3), the long-term modulus E_∞ corresponds to the elastic behavior under quasi-static deformation ($\omega \to 0$). It should be emphasized that a complex shear modulus G^* is often used in the literature to represent the material properties. Under the assumption of isotropy and using the Poisson's ratio ν, the following relationship prevails

$$E^* = 2G^*(1+\nu). \tag{5}$$

Due to the chemical composition of viscoelastic materials such as elastomers, an analogy exists between the frequency and temperature dependence. The mechanical behavior at low frequencies is similar to that at high temperatures and vice versa. This phenomenon, known as time-temperature superposition, allows for shifting the frequency-dependent material curves and thus determine the material properties at arbitrary temperatures. For rheological simple materials, the shift along the frequency axis can be performed by a horizontal shift factor a_T, which results from the WLF equation [5]

$$\log(a_T) = \frac{-C_1 \cdot \Delta T}{C_2 + \Delta T}, \tag{6}$$

where the parameters C_1 and C_2 are fitting parameters and ΔT is the difference between the actual and the reference temperatures ($\Delta T = T - T_{\mathrm{ref}}$). For instance, the loss modulus at a reference temperature T_{ref} and at a reference frequency f_{ref} is the same as at any temperature T and at a frequency $f = a_T \cdot f_{\mathrm{ref}}$. If the elastomer is filled with carbon black, the Payne effect [3,4] occurs, which is included in the time-temperature analogy by an additional vertical shift. The vertical shift is considered as an Arrhenius-like activation process and the corresponding shift factor b_T can be calculated from the apparent activation energy E_A, the universal gas constant R and Euler's number e [45]

$$b_T \approx \mathrm{e}^{-\frac{E_A}{R \cdot \Delta T}}. \tag{7}$$

Finally, the material properties at any temperature and frequency can be determined by incorporating both shift factors

$$E^{'}(f, T) \to b_{T,E^{'}} \cdot E^{'}\left(a_T \cdot f_{\mathrm{ref}}, T_{\mathrm{ref}}\right)$$

$$E''(f, T) \to b_{T,E''} \cdot E''\left(a_T \cdot f_{\mathrm{ref}}, T_{\mathrm{ref}}\right). \tag{8}$$

It should be noted that the activation energies for storage and loss modulus may be different. For more detailed information on the chemical background and the application of the shift process, the interested reader is referred to [46].

2.2. Analysis method

The eigenvalue problem of a system which is composed of elements with frequency-dependent viscoelastic properties is of nonlinear nature [47]

$$\left[\mathbf{K}^*\left(\lambda_r^*\right) - \lambda_r^{*^2}\mathbf{M}\right]\phi_r^* = 0, \tag{9}$$

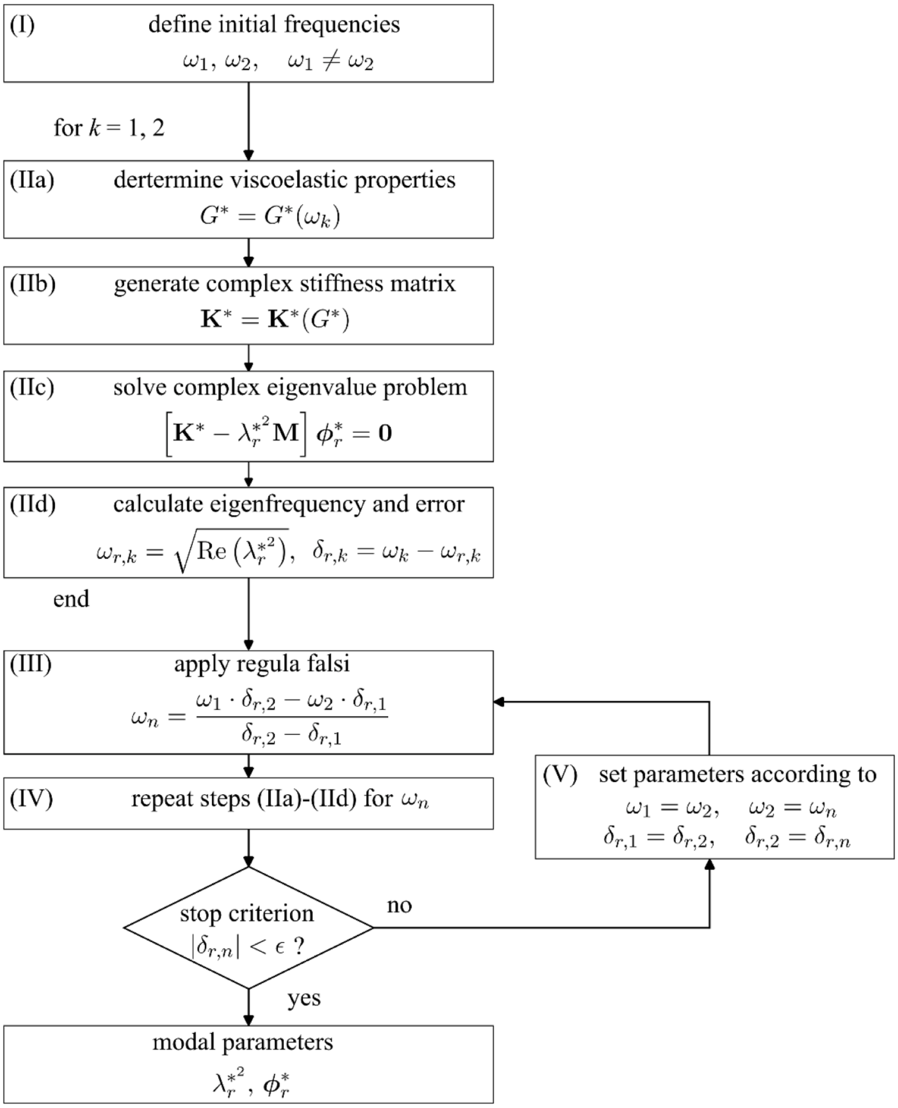

Fig. 1. Algorithm of the iterative eigenvalue solver.

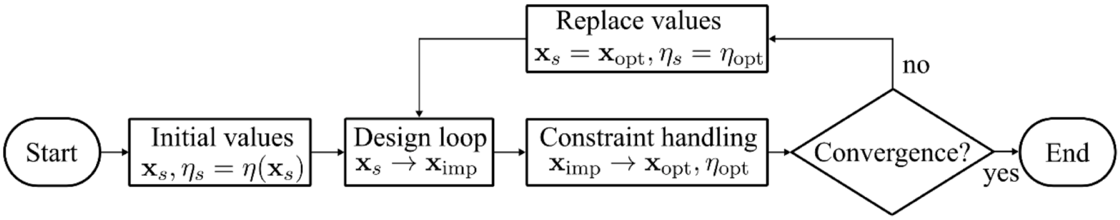

Fig. 2. Basic flowchart of the optimization algorithm.

where $\mathbf{M}$ denotes the mass matrix, $\mathbf{K}^*$ the complex stiffness matrix, λ_r^* the complex eigenvalue of mode r and ϕ_r^* the corresponding complex eigenvector. The complex nature of the stiffness matrix is due to the complex viscoelastic properties propagating through the FE formulation. More information on the composition of the complex stiffness matrix can be found in [46]. It should be noted that the complex eigenvalue resulting from a viscoelastically damped system has to be interpreted differently than the eigenvalue of a viscously damped vibration. For viscoelastic damping the eigenvalue is defined as [47]

$$\lambda_r^{*^2} = \omega_r^2(1 + \mathrm{i}\eta_r). \tag{10}$$

Basically, the real part contains the information about the eigenfrequency ω_r, while the damping in terms of the modal loss factor η_r is obtained by the ratio of imaginary and real part

$$\eta_r = \frac{\mathrm{Im}\left(\lambda_r^{*^2}\right)}{\mathrm{Re}\left(\lambda_r^{*^2}\right)}. \tag{11}$$

It is worth to emphasize the difference between the modal loss factor and the material loss factor. While the modal loss factor η_r denotes the damping of the mode of a system and is thus a system property, the material loss factor $\tan(\delta)$ indicates the material damping capacity which is independent of the properties of the system where this material is applied. Furthermore, for weakly damped systems, an analogy exists to the viscous damping ratio D_r by $2D_r \approx \eta_r$. This relationship will be used later to compare the numerical and experimental results.

From eq. (9) and (10) it can be concluded that the eigenvalue problem is not directly solvable due to the frequency-dependent stiffness matrix. However, this difficulty can be circumvented by using appropriate analysis methods. Some of these methods are reported and reviewed by Vasques et al. [12] and compared by Rouleau et al. [47]. In the following section, we will apply an iterative eigenvalue solver (IES) whose constitutive algorithm is based on the *regula falsi* method and has already been part of studies in [46,48]. Fig. 1 shows the basic procedure of the IES.

At first, two initial frequencies are defined (I). For each of these frequencies, the viscoelastic material properties are determined (IIa), the complex stiffness matrix is generated (IIb) and the linear complex eigenvalue problem is solved (IIc). Afterwards, the corresponding eigenfrequencies are computed and the absolute error δ_r between the initial frequency and the eigenfrequency is calculated (IId). The results are transferred to the *regula falsi* method, where an optimized frequency is estimated (III). In step (IV), the previous steps (IIa) – (IId) are repeated for the optimized frequency. If the stop criterion (threshold ε) does not apply, the parameters are changed as described for step (V). Otherwise, the eigenvalue and eigenvector are found and the modal loss factor can be computed by eq. (11).

3. A new approach for shape optimization of CLD beams

This section deals with the theory of the chosen optimization technique and introduces the corresponding algorithm. For a better overview, the algorithm is divided into two parts: the design loop and the mass constraint handling. An illustrative example is given at the end of this section.

3.1. Formulation of the structural optimization problem

The objective of the optimization approach is to maximize the damping of a vibrating CLD beam by finding the optimal width distribution of the core and face layers with respect to predefined mass and geometrical constraints. The FE mesh of the host structure is kept constant during the optimization with a fixed number of elements in the longitudinal and transverse directions. Additionally, a symmetry axis is assumed along the longitudinal axis. Starting from the symmetry axis, finite elements of the viscoelastic core and the metallic face layer are simultaneously added to the left and to the right of the symmetry axis, while each element group in longitudinal direction defines a potential design variable x_j. For instance, a value of $x_j = 0$ means that no CLD material is added and a value of $x_j = 2$ adds two CLD elements left and right of the symmetry axis. An advantage of this approach is that several elements can be combined as one design variable, thus reducing the computational effort. Moreover, symmetry effects of the vibration modes can be used to further simplify the problem. An example of this procedure will be shown later in Section 3.5. The general optimization problem can be expressed as a minimization problem

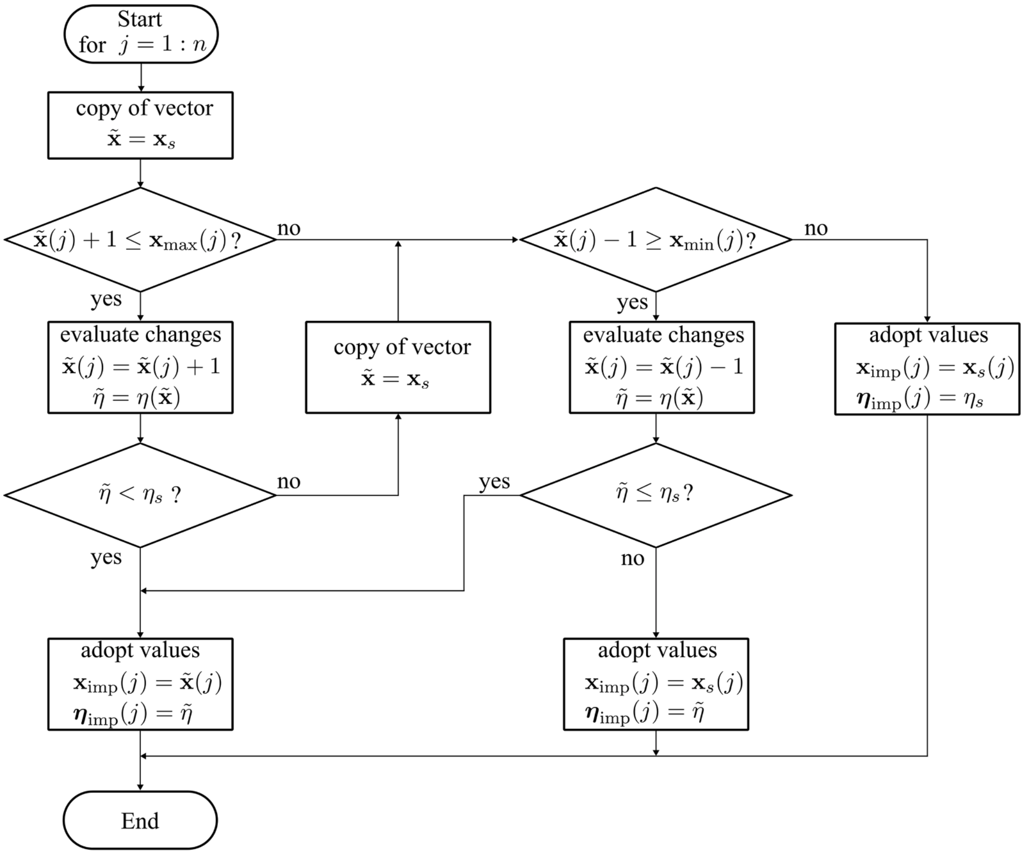

Fig. 3. Flowchart of the design loop algorithm.

$$
\begin{aligned}
\text{Minimize :}\quad & -\eta(\mathbf{x}) \\
x_j \in \mathbb{N}_0 & \\
\text{Subject to :}\quad & m_{\mathrm{CLD}}(\mathbf{x}) - m_{\mathrm{bound}} \leq 0 \\
& x_{\min} \leq x_j \leq x_{\max}, \qquad \text{for } j = 1, \ldots, n
\end{aligned}
\tag{12}
$$

where m_{CLD} is the actual mass of the system, m_{bound} is the permitted mass, $\mathbf{x}$ is the vector of n design variables x_j and $x_{\min}$ and $x_{\max}$ are geometrical limits. Due to the discrete FE mesh, the design variables can only be zero or positive integer numbers.

3.2. Basic structure of the optimization algorithm

Fig. 2 shows the basic structure of the applied algorithm. In general, the presented method can be divided into two parts: The design loop and the mass constraint handling. The algorithm starts with the initial design variables $\mathbf{x}_s$ and the corresponding objective function value η_s. As a first step, this data set is utilized in the design loop to find improved design variables $\mathbf{x}_{\mathrm{imp}}$. The improved data set is passed to the mass constraint handling, which checks for mass constraint violations and eventually modifies the improved data set. Afterwards, the optimal design variables $\mathbf{x}_{\mathrm{opt}}$ are available and the results are checked for convergence.

The evaluation of the objective function $\eta(\mathbf{x})$ triggers two subprocesses. First, the FE mesh is regenerated according to the design variable vector. Then, the corresponding eigenvalue problem is solved. When considering frequency-dependent viscoelastic properties, the IES shown in Fig. 1 is applied. Due to the geometrical modifications, mode switches may occur during the optimization. This means, for example, that a bending mode and a torsion mode change the order of appearance. In order to track the mode of interest, it is recommended to compare the resulting mode shapes of the eigenvalue analysis to a reference mode shape. The Modal Assurance Criterion (MAC) is an appropriate tool for this purpose [49].

3.3. Design Loop

The key part of the algorithm is the design loop shown in Fig. 3. The principle of the design loop is based on the Gauss-Seidel method. For each step in the for-loop, a copy $\tilde{\mathbf{x}}$ of the initial design vector is created. It is then checked whether increasing the j^{th} design variable violates the associated maximum geometric limit. If not, the change is accepted and the modified design variables are

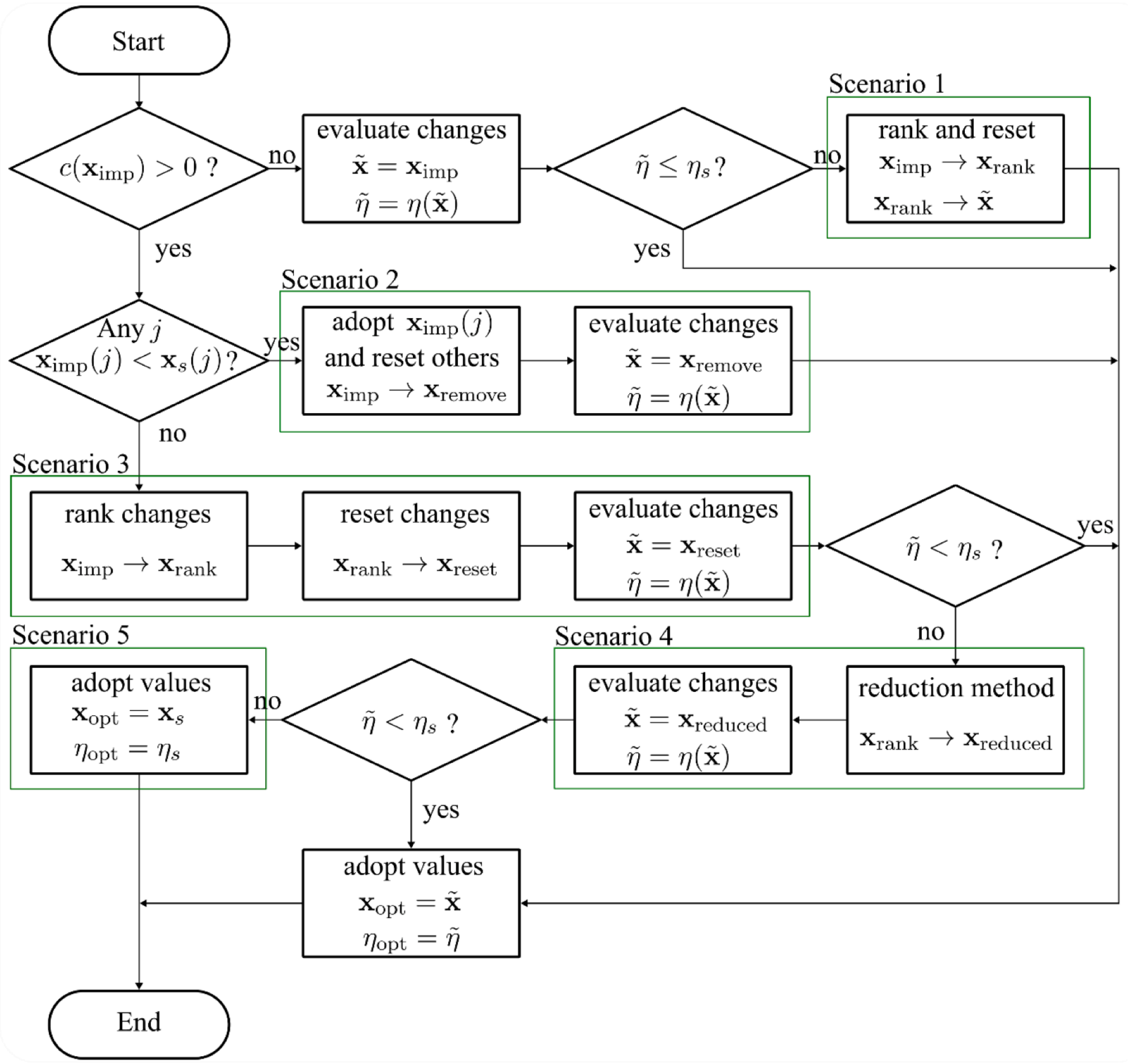

Fig. 4. Flowchart of the mass constraint handling.

evaluated in the objective function, resulting in a temporary value of the modal loss factor $\tilde{\eta}$. In case the change yields an improvement of the objective function value, both values are stored in the corresponding vectors $\mathbf{x}_{\text{imp}}$ and $\boldsymbol{\eta}_{\text{imp}}$ for later use. If no improvement is achieved, or if an increase of a design variable violates the upper geometric limit, it is checked whether a reduction of the design variable value is feasible. If this is true and if the modified design yields an improvement, the changes are accepted and saved. If either of these conditions is false, the changes are discarded and the initial values are adopted. At the end of the loop, the vector $\mathbf{x}_{\text{imp}}$ contains all individual geometric modifications, while the vector $\boldsymbol{\eta}_{\text{imp}}$ contains the associated modal loss factors. It should be noted that the part in Fig. 3 denoted as *evaluate changes* actually means the analysis of the FE model with the current design vector. This is the computationally intensive part of the optimization.

3.4. Mass constraint handling

Five different scenarios can occur during the mass constraint handling. The corresponding flowchart is shown in Fig. 4 and the scenarios are described below. The mass constraint function is denoted as $c(\mathbf{x})$.

1. **Constraint is not violated**

If the mass constraint is not violated, it is still necessary to check whether the simultaneous application of all single improvements leads to an improvement of the modal loss factor. If it does, the geometric changes are accepted. If not, scenario 1 applies. Within this scenario, the improvements of the single modifications are ranked according to their impact on the modal loss factor and the

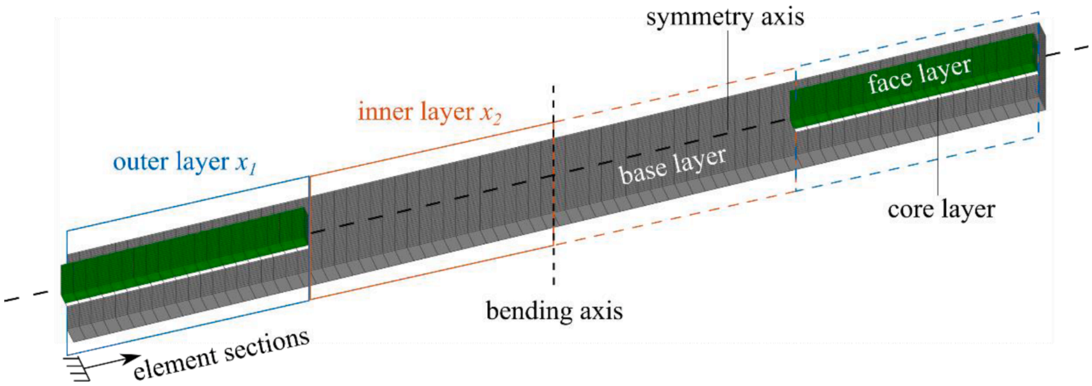

Fig. 5. Initial design of the CLD beam and definition of the inner and outer layers. The white layer corresponds to the viscoelastic core layer, while the face layer is colored in green. (For interpretation of the references to colour in this figure legend, the reader is referred to the web version of this article.).

Table 1
Properties of the CLD layers.

	Density (kg/m^3)	Storage modulus (GPa)	Poisson's ratio (-)	Material loss factor (-)	Thickness (mm)
Base layer	2660	70	0.33	0.005	8
Core layer	1114	0.1	0.499	0.4	2
Face layer	2660	70	0.33	0.005	5

modifications are reset sequentially, starting with the worst improvement. This loop is stopped when an improvement of the objective function value is achieved.

2. **Constraint is violated and the value of at least one design variable is reduced**

If the mass constraint is violated, it is checked if the value of any of the improved design variables is lower compared to the initial step. This would mean that elements are removed and the mass condition is inevitably satisfied. In this case, the corresponding design variable is accepted and all other improvements are discarded ($\mathbf{x}_{\text{imp}} \rightarrow \mathbf{x}_{\text{remove}}$). If the above-mentioned condition applies to more than one design variable, all of these design variables are temporarily accepted. However, the simultaneous adoption of multiple design variables may cause the modal loss factor to decrease and needs to be verified. If an improvement is confirmed, the adoption is valid. Otherwise, only the modification providing the best improvement of the modal loss factor is adopted.

3. **Constraint is violated and no value of any design variable is reduced**

If the improved design vector does not result in an elimination of any elements, the design changes are ranked according to their improvement of the modal loss factor ($\mathbf{x}_{\text{imp}} \rightarrow \mathbf{x}_{\text{rank}}$). Afterwards, the increase of each design variable is reset, starting with the worst. This procedure is repeated until the mass condition is satisfied ($\mathbf{x}_{\text{rank}} \rightarrow \mathbf{x}_{\text{reset}}$). If the resulting configuration is an improvement over the initial state, the design variables are accepted.

4. **Constraint is violated, removal of individual design variables did not yield an improvement**

Scenario 4 works as follows: A reduction technique is applied based on the ranked design variable vector $\mathbf{x}_{\text{rank}}$. For this purpose, only the design variable leading to the best improvement is kept and the others are discarded and return to the initial state of the loop. Then the worst design variable x_w, which corresponds to the design variable providing the least improvement, is treated as a free parameter, while the other design variables are fixed. As a consequence, the mass constraint condition is transformed into a single variable function $(c(\mathbf{x}) \rightarrow c(x_w))$ and the worst design variable is systematically reduced by

$$x_{w,k+1} = x_{w,k} - 1 \tag{13}$$

until the mass condition is satisfied. In eq. (13), k indicates the k$^{\text{th}}$ step within the reduction method. The new design vector is evaluated and it is checked whether an improvement is achieved. If not, the second worst design variable is selected as a free parameter and the reduction method is applied again. The same applies if a design variable exceeds the lower bound in the course of

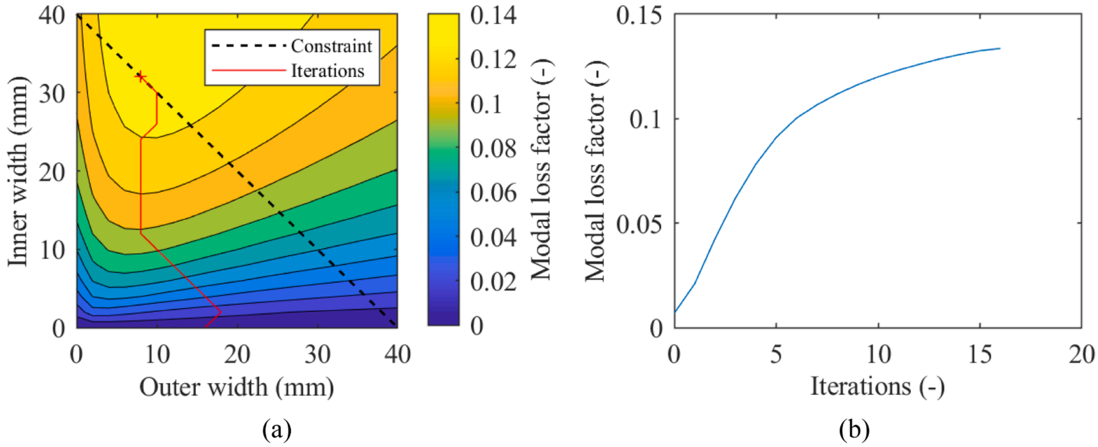

Fig. 6. (a) Iteration path from start point to maximum and (b) corresponding convergence diagram.

Fig. 7. Top: Optimal design of the first bending mode from top view. Black color indicates added core and face layers. Bottom: Mode shape of the first bending mode.

the reduction method. This procedure is repeated until the (n-1)$^{\text{th}}$ worst design variable or until an improved modal loss factor is obtained. Finally, the improved values are adopted as optimal parameters.

5. **Constraint is violated and reduction method does not yield a feasible improvement**

If the constraint is violated and the reduction method does not lead to a feasible improvement, the initial values are adopted as optimal values and the algorithm is terminated.

3.5. Illustrative example

An example with two design variables is presented in the following to demonstrate the application of the optimization approach to a free-free vibrating CLD beam structure. MSC Nastran is used as the FE solver and the algorithm introduced in the previous section is implemented in MATLAB. For the purpose of this example, the objective is to maximize the modal loss factor of the first bending mode. Additionally, a constraint is defined, limiting the coverage of the CLD material to 50 % of the top surface of the beam. Since the first bending mode is symmetric with respect to the bending axis, the symmetry is used to reduce the number of design variables and thus the numerical effort. As a result, two design variables x_1 and x_2 represent the width of the inner and outer layers, respectively. As illustrated in Fig. 5, both segments have the same size. The structure is regularly meshed by 80 CHEXA solid elements in the longitudinal direction (400 mm) and 40 elements in the transverse direction (40 mm) with one element per layer in the thickness direction. It follows that x_1 contains element sections 1-20 and 61-80 and x_2 contains element sections 21-60. Perfect bonding is assumed, which means that the geometrical influence of the adhesive layer as well as bonding failure is neglected and elements of adjacent layers share the same nodes.

The properties of the composite structure are listed in Table 1. In this example, the properties of the viscoelastic layer are kept constant. This assumption differs from real material behavior, but is considered as acceptable for the demonstration of the algorithm. Furthermore, the analyses in this paper are performed under the assumption of small vibrations. As a consequence, the expected strains and displacements are small, so that amplitude-dependent effects of the applied materials are negligible. It should also be noted that core and face layer elements are always added or removed together and do not overlap the base layer.

The initial design vector is $\mathbf{x}_s = [8 \quad 0]^{\mathrm{T}}$. Due to the line of symmetry in the longitudinal direction, the design variables correspond to a width of 16 mm for the outer layer and 0 mm for the inner layer. Fig. 6 (a) shows the iteration path with the corresponding convergence diagram (b). The optimization ends after 17 iterations with an optimal design vector of $\mathbf{x}_{\mathrm{opt}} = [4 \quad 16]^{\mathrm{T}}$ and a modal loss

Fig. 8. Optimal design resulting from the optimization with (a) four and (b) eight variables.

Table 2
Optimization results for different numbers of design variables.

Variables (-)	Modal loss factor (-)	Increase (%)	Obj. function calls (-)	Optimal design vector (-)
2	0.1336	-	62	[4 16]
4	0.1394	4.34	121	[1 8 13 18]
8	0.1405	5.17	221	[0 3 6 9 12 15 17 18]

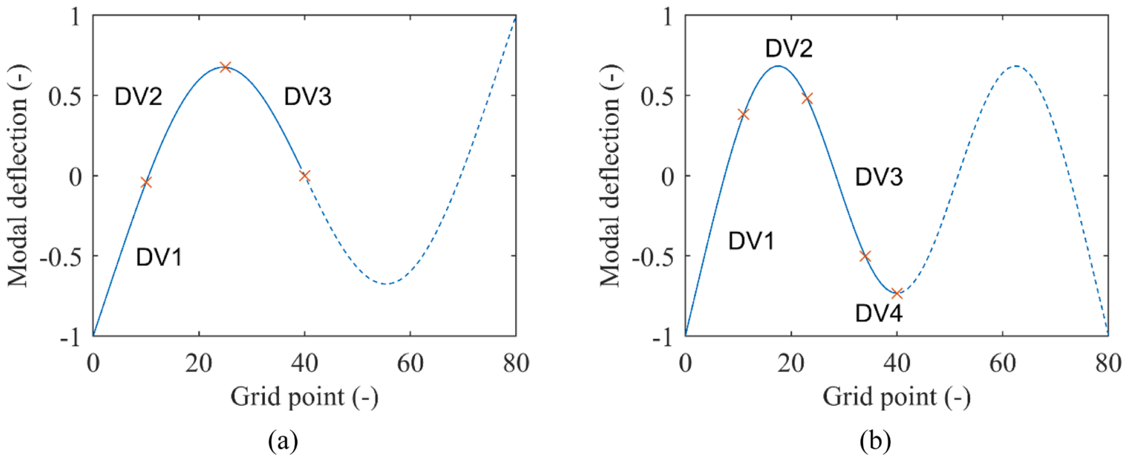

Fig. 9. Modal bending deflection of (a) the second and (b) the third bending mode. Red markers indicate the position of the design variable (DV) separation. In this context, (a) shows the DV separation of approach (1), while (b) shows the DV separation of approach (2).

factor of $\eta_{\text{opt}} = 0.1336$. The optimal widths are 8 mm for the outer layer and 32 mm for the inner layer, as illustrated in Fig. 7.

It can be seen in Fig. 6 (a) that the optimal solution conforms with the solution of the contour plot. Moreover, the allowed mass increase is fully utilized. The reason for the resulting CLD shape can be explained as follows: Shear deformation is crucial to activate the damping properties of the viscoelastic material. In the case of the first bending mode, the highest shear strain occurs at the outer edges of the viscoelastic layer and is termed as the *edge effect* by Lepoittevin and Kress [32]. High shear deformation is achieved by a flexible viscoelastic layer. However, if the shear stiffness of the viscoelastic layer is too flexible, the corresponding strain energy is much lower than the strain energy of the base and face layers. As a consequence, only a small portion of the strain energy can be dissipated through the viscoelastic material, resulting in poor damping. On the other hand, if the layer is too stiff, the opposite effect occurs. As the shear stiffness increases, the shear deformation of the viscoelastic layer decreases and the corresponding strain energy is low compared to the strain energy of the elastic layers.

In order to achieve high damping performance, it is therefore necessary to find a compromise between high shear strain and adequate shear stiffness. As presented in [46], the shear stiffness of the viscoelastic layer depends on the length, width and thickness of the layer as well as on the shear storage modulus of the viscoelastic material. Accordingly, the shear stiffness can be enhanced by increasing the material stiffness (storage modulus) or by increasing the width and length of the layer, but also by decreasing the thickness of the layer. In the present example, the viscoelastic material stiffness appears to be relatively high, so that the effect on the shear stiffness is compensated by slender core and face layers at the outer edges of the beam. Later, in Section 5.1, it will be demonstrated that the optimal design changes with the viscoelastic material stiffness.

4. Characteristics of the optimization approach

This chapter discusses some characteristics and the performance of the optimization approach. The influence of the number and distribution of design variables on the optimized design and on the modal loss factor is analyzed. The meshed beam structure from Section 3.5 serves as the basis for the analyses. Unless otherwise specified, the material properties, geometric dimensions and assumptions given in Section 3.5 are adopted. A performance comparison with other CLD placement strategies is presented at the end of this section.

4.1. Influence of the number of design variables on optimization results

In Section 3.5, the optimization was performed with two design variables to maximize the damping of the first bending mode. In the following, it is analyzed if increasing the number of design variables improves the optimization results. Finally, it is examined whether

Table 3
Design variable definition and modal loss factor for the second bending mode.

Approach	Included element sections (-)				Modal loss factor (-)
	DV1	DV2	DV3	DV4	
(1)	1-10 + 71-80	11-25 + 56-70	26-55	-	0.1144
(2)	1-5 + 76-80	6-16 + 65-75	17-34 + 47-64	35-46	0.1136
(3)	1-10 + 71-80	11-20 + 61-70	21-30 + 51-60	31-50	0.1150

Table 4
Design variable definition and modal loss factor for the third bending mode.

Approach	Included element sections (-)				Modal loss factor (-)
	DV1	DV2	DV3	DV4	
(1)	1-7 + 74-80	8-18 + 63-73	19-28 + 53-62	29-52	0.0811
(2)	1-11 + 70-80	12-23 + 58-69	24-34 + 47-57	35-46	0.0862
(3)	1-10 + 71-80	11-20 + 61-70	21-30 + 51-60	31-50	0.0845

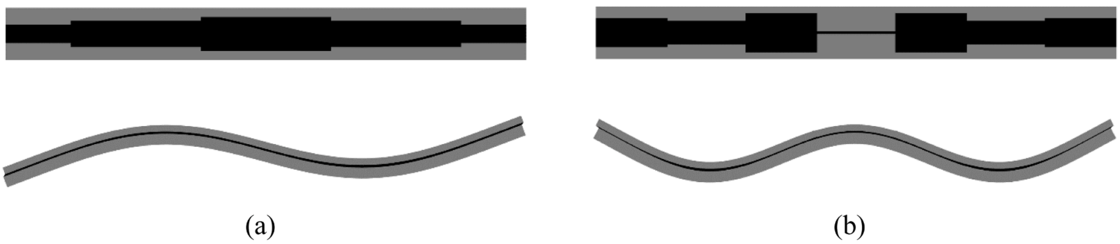

Fig. 10. Optimal design of (a) the second and (b) third bending mode from top view with the corresponding mode shapes.

the increased numerical effort is justified. For this purpose, the beam is divided into four and eight equally spaced sections that are symmetrically positioned around the symmetry axis. This means that in the case of four design variables, each design variable contains 10 element sections. Since the path of the optimization depends strongly on the initial values, the starting position is always the uncovered beam ($\mathbf{x}_s = \mathbf{0}$). The optimized designs are presented in Fig. 8 (a) and (b) and the corresponding modal loss factors and the number of objective function calls are listed in Table 2.

From Fig. 8 it can be seen that in both cases an elliptical shape for the optimal design emerges as the number of design variables is increased. The result can be easily compared to Fig. 7, which shows the result with only two design variables. Most of the CLD material is added at locations of maximum bending moment (center of the beam), where the modal strain energy of the host structure is also maximum. This is consistent with the approach of Kumar and Singh [42,43], who added single CLD patches at locations of highest modal strain energy. However, the computational cost increases significantly. Doubling the number of design variables roughly doubles the number of objective function calls. On the other hand, the modal loss factor increases only slightly. Compared to two design variables, eight variables cause a relative damping increase of 5.17 %. A compromise might be to start with a small number of variables and continue the optimization with an increased number when convergence is achieved. Alternatively, shape interpolation can be a useful tool to keep the numerical effort low while still approaching an optimal design.

4.2. Influence of the design variable distribution on optimization results

Another question is the applicability of the previous method to higher modes. Basically, the first bending mode shape of the beam in free-free boundary conditions is similar to a half-sine. However, the mode shapes of higher modes become more intricate. In this case, it also seems necessary to increase the number of design variables and to rethink their distribution on the FE structure. This task is addressed in this section. For the second and third bending mode, three different distribution approaches for the design variables are analyzed:

(1) Separation at vibration nodes and antinodes
(2) Distribution on vibration nodes and antinodes
(3) Distribution according to equal element size (as shown in Section 3.5)

In this regard, Fig. 9 shows the bending deflection of the uncovered beam for the second and third modes as a function of the grid points in the longitudinal direction. It should be noted that the second bending mode is point symmetric with respect to the center point, while the third mode is mirror-symmetric. In this context, Table 3 and Table 4 list the element sections that belong to the corresponding design variables for the three different distribution approaches.

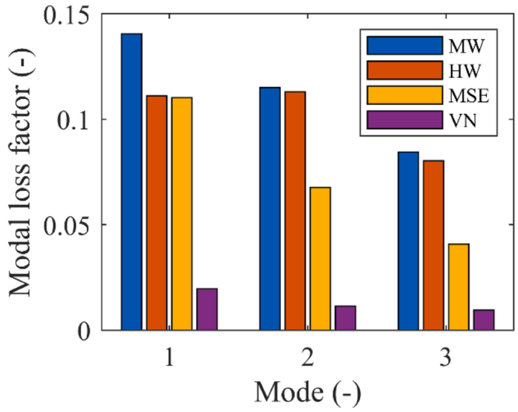

Fig. 11. Modal loss factor of first three bending modes resulting from different placement strategies: The proposed multiple width approach (MW), uniform half-width placement (HW), placement of CLD patches at maximum modal strain energy (MSE) positions and at vibration nodes (VN).

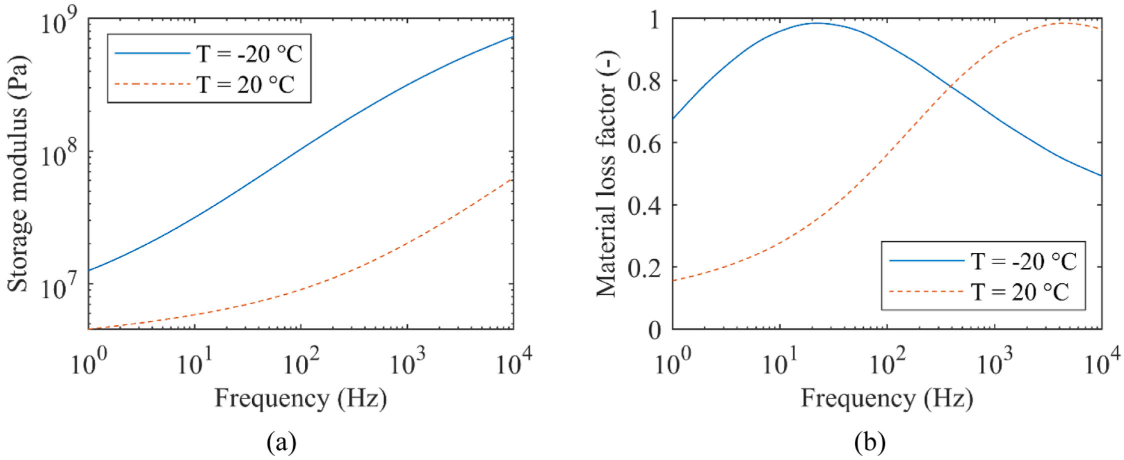

Fig. 12. (a) Shear storage modulus and (b) loss factor of BIIR at -20°C and 20°C.

As shown in Table 3, the highest modal loss factor for the second bending mode can be achieved when the distribution approach (3) with $\mathbf{x}_{\mathrm{opt}} = [7\ 10\ 10\ 13]^T$ is applied. In contrast, the distribution approach (2) with $\mathbf{x}_{\mathrm{opt}} = [11\ 9\ 15\ 1]^T$ is the most promising for the third bending mode. The corresponding final designs are shown in Fig. 10.

The optimal design for the second bending mode also suggests an elliptical shape. The highest shear strain in the viscoelastic layer occurs at the free ends and in the center. While the layer width is small at the outer edges, it increases towards the center. In contrast, the optimal design for the third bending mode exhibits slimmest layers at the antinodes. In particular, the design at the central antinode is remarkable because an extremely thin section appears. However, this section is not redundant - removing it reduces the modal loss factor relatively by 2.44 %. Instead, the core and face layers are wider at the free ends and between the antinodes. It should be noted that the width at the outer edges increases for higher modes. This is due to the fact that the mode shape becomes more intricate, which also increases the strain energy in the elastic layers. To ensure a high ratio of modal strain energies, the shear stiffness of the visco-elastic layer must be enhanced. This is achieved by adding CLD material at the location of maximum shear deformation.

4.3. Comparison to other CLD placement approaches

To demonstrate the effectiveness of the proposed optimization approach, a comparative study with other placement strategies is performed under the same mass conditions (50 % surface coverage). One approach is to cover the full length of the beam with half the width of the CLD layers. The other two strategies include placing CLD patches at vibration nodes, as e.g. performed in [41], and at positions of highest modal strain energy, following the ideas proposed in [42,43]. Maximum modal strain energy is typically located at antinodes. Fig. 11 compares the modal loss factors of the first three bending modes, resulting from the four approaches. The proposed optimization approach provides the highest damping for all modes. It is particularly superior (e.g. up to 52 % to the MSE approach) to the mode shape-based placement strategies.

Table 5
Comparison of optimal designs and modal loss factors for different storage moduli.

Mode	Config.	Optimal design	Modal loss factor (-) $E' = 0.1$ GPa	Modal loss factor (-) $E' = 0.01$ GPa
1.	A		0.1394	0.0566
	B		0.0802	0.0816
2.	A		0.1150	0.0295
	B		0.0733	0.0371
3.	A		0.0868	0.0202
	B		0.0622	0.0205

Table 6
Design variable distribution for the third bending mode.

DV1	DV2	DV3	DV4
1-5 + 76-80	6-11 + 70-75	12-17 + 64-69	18-23 + 58-63
DV5	DV6	DV7	DV8
24-28 + 53-57	29-34 + 47-52	35-37 + 44-46	38-43

5. Application of the optimization approach under real conditions

In this chapter, the application of the proposed optimization approach is demonstrated by means of a CLD beam with a real viscoelastic material. The damping material is a bromobutyl rubber blend (BIIR), which has been used in previous studies [46,50,51]. The frequency- and temperature-dependent material behavior is fully characterized by Prony, WLF and Arrhenius parameters, as shown in Tables A.1 and A.2 in the Appendix. Two different temperatures (T_1 = -20°C and T_2 = 20°C) are chosen for the design optimization. These temperatures are representative of the airframe temperature of a large transport aircraft during a flight. The upper thermal boundary represents the temperatures on the ground. The lower thermal boundary considers the ambient temperature at flight altitude with some frictional heating from the boundary layer around the airframe when flying at transonic speed. Fig. 12 shows the storage modulus and the material loss factor as a function of frequency for both temperatures.

As depicted in Fig. 12, both storage modulus and loss factor vary considerably with frequency and temperature. The material stiffness is low at low frequencies and also at high temperatures. In contrast, the loss factor has a maximum at low frequency for -20°C and at high frequency for 20°C. The region of significant stiffness change and highest loss factor is typically referred to as the glass transition region of the elastomer material.

In particular, the storage modulus is a key parameter for achieving the highest damping. However, there is no rule of thumb for a rough estimation of a suitable scale for the storage modulus, since it depends strongly on the dimensions of the composite structure and its mode shapes. As shown by Gröhlich et al. [46], an inappropriate viscoelastic storage modulus can be compensated by geometric adaption of the CLD layers. In contrast, the material loss factor can be understood as a proportional factor for tuning the damping of a vibrating system: high loss factors lead to high vibration damping.

5.1. *Design dependence on storage modulus*

Since material loss factor and storage modulus are coupled parameters in real elastomeric materials and change simultaneously with temperature and frequency, it is difficult to clearly distinguish the dominant parameter. Therefore, in order to distinguish between the impacts of both material parameters, the influence of a storage modulus variation on the optimized design is considered in this section. For this purpose, the storage modulus of the viscoelastic material is expressed as a constant value of $E' = 0.01$ GPa and $E' = 0.1$ GPa, respectively. As shown in Fig. 12, it is possible to have a modulus variation by a factor of 10 in the considered temperature range. The other properties remain as in Table 1. For the first and second bending modes, the element distribution approach (3) of Section 4.2 is applied and for the third mode, the element distribution approach (2) is taken. The final designs, called configuration A for $E' = 0.1$ GPa and configuration B for $E' = 0.01$ GPa, are presented and compared in Table 5.

Comparing the first modes, the design for the lower storage modulus (configuration B) is inverted. The elliptical shape changes to an hourglass-like shape, where most of the CLD material is added at the free end of the beam and less material is added at the location of maximum bending moment and maximum modal strain energy, respectively. This observation can be physically explained with the same explanation given in Section 3.5. Due to the lower viscoelastic material stiffness, the decrease in the shear stiffness of the layer is

Table 7
Comparison of optimal designs and modal loss factors at different temperatures.

Mode	Config.	Optimal design	Modal loss factor (-) T = -20°C	Modal loss factor (-) T = 20°C
1.	C		0.2122	0.0720
	D		0.0972	0.1572
2.	C		0.2128	0.0641
	D		0.1051	0.1080
3.	C		0.1892	0.0563
	D		0.0970	0.0792

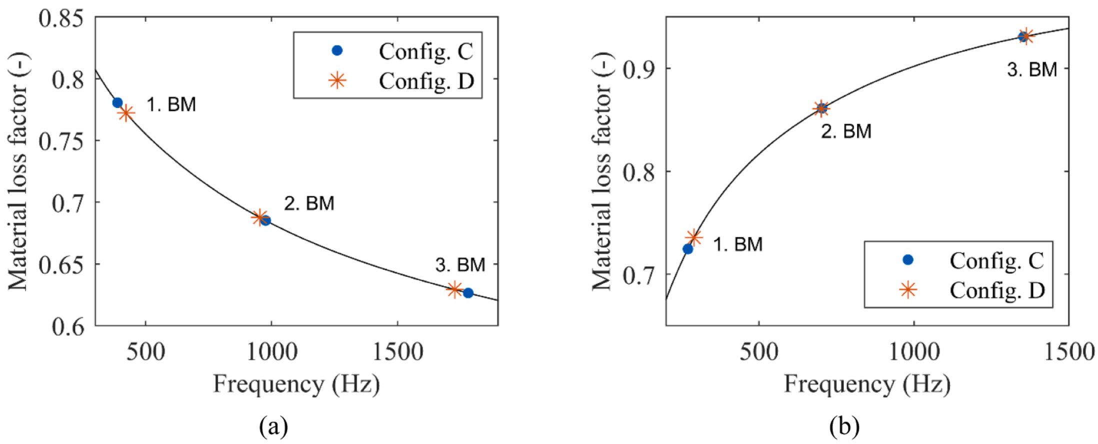

Fig. 13. Material loss factors at eigenfrequencies of first three bending modes (BM) at (a) -20°C and (b) 20°C. It should be noted that the horizontal axis is plotted in linear scale.

compensated by wider layer sections at the locations of maximum shear strain. The same applies to the second and third modes. Compared to configuration A, the sections of maximum shear deformation are widened, while the section corresponding to the antinodes is thinned. The central element disappeared completely for the third mode. Instead, two thin rods appear on top of the outer antinodes, forcing the adjacent wider damping patches into shear strain.

An important observation can be made by looking at the modal loss factor. CLD designs are less efficient when the viscoelastic storage modulus differs from the value that has been assumed for the design optimization. For instance, using design 1B instead of 1A for a viscoelastic storage modulus of 0.1 GPa, results in 42.5 % less damping. On the other hand, using design 1A instead of 1B for a storage modulus of 0.01 GPa, the modal loss factor is also 30.6 % less. An exception can be observed for the third mode. Here, the inappropriate design (configuration 3A) provides almost the same damping for $E^{'} = 0.01$ GPa as the appropriate design (configuration 3B). The analysis shows that the final design of a CLD treatment is not only mode-dependent, but also strongly dependent on the prevailing viscoelastic storage modulus.

5.2. Thermal influence on optimal design

In this section, the material properties presented in Fig. 12 are applied to the viscoelastic material. An optimization is performed for the two temperatures mentioned above. For this purpose, the IES has to be implemented in the process chain. Additionally, the number of design variables is set to eight. This means that for the first and second bending mode (distribution approach (3)), each design variable contains ten elements (e.g. DV1: 1-5 + 76-80). The distribution for the third bending mode follows approach (2) with a distribution scheme shown in Table 6.

The results of the optimization runs are presented in Table 7. Configuration C corresponds to a layout temperature of -20°C, while configuration D corresponds to a temperature of 20°C. It can be seen that the designs for both configurations are almost opposite. This is especially true for the first and second modes. For example, the optimal design of the first mode changed from a *rolling pin* shape to a *dumbbell* shape at a higher temperature.

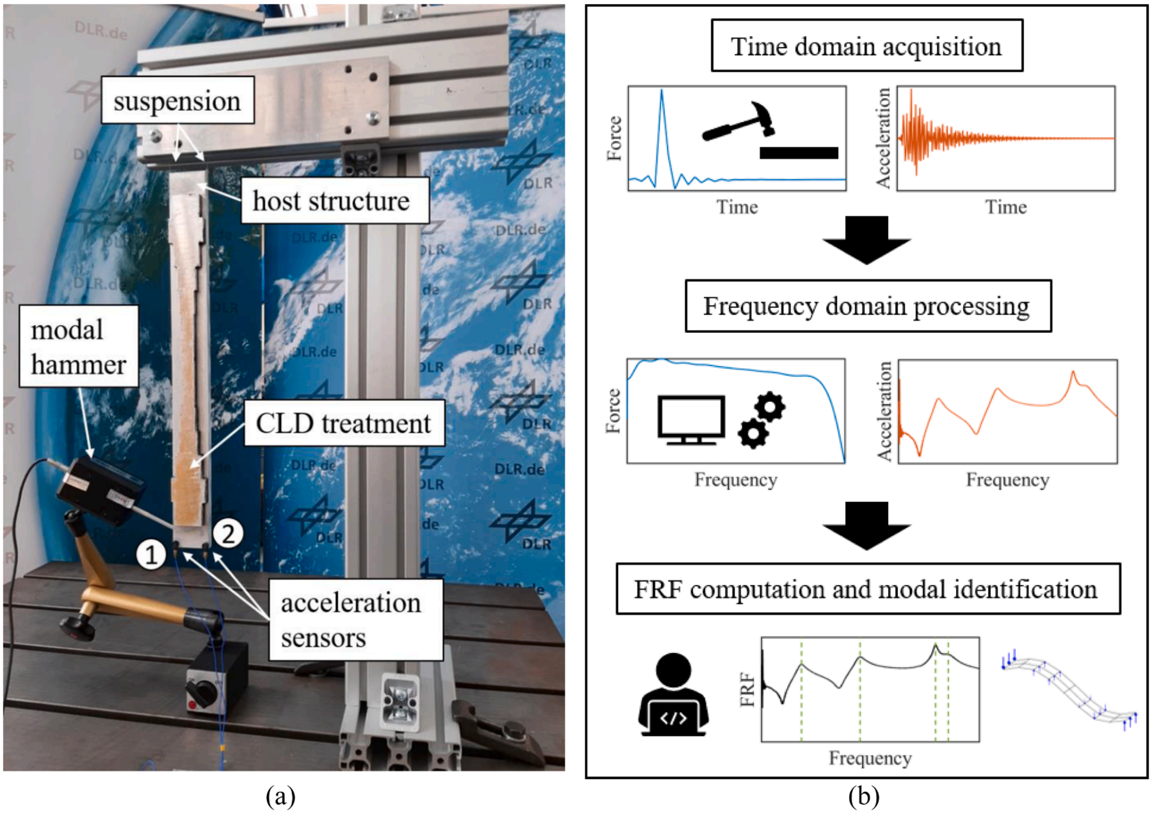

Fig. 14. (a) Experimental setup of the impact test and (b) process chain of experimental modal analysis.

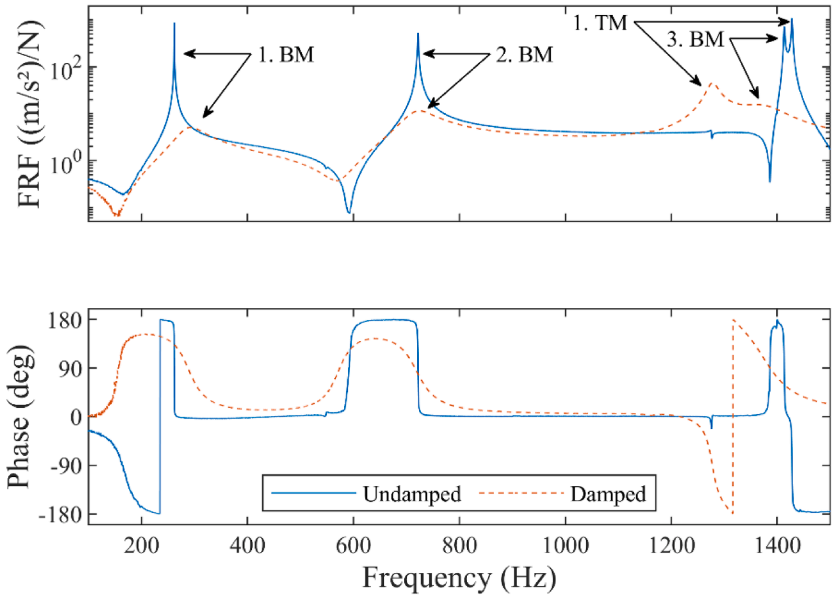

Fig. 15. Bode plot of Sensor 2 for the undamped and damped beam.

Table 8
Comparison of simulation and experimental data of the bending modes.

Mode	Modal parameter	Simulation	Experiment	Deviation (%)
1. bending mode	Eigenfrequency (Hz)	291.4	289.2	0.76
	Damping (%)	7.92	8.51	-6.93
2. bending mode	Eigenfrequency (Hz)	719.9	719.1	0.11
	Damping (%)	3.90	4.11	-5.11
3. bending mode	Eigenfrequency (Hz)	1377	1376	0.07
	Damping (%)	2.99	3.13	-4.47

The modal loss factor values underscore the observations made in Section 5.1: The design optimized for a specific temperature provides significantly less damping performance when operated at a different temperature. Looking at Fig. 13, it is evident that this effect is not primarily caused by different material loss factors, prevailing at the corresponding eigenfrequencies. At -20°C (a), the material loss factor of the second and third bending modes (BM) of configuration C is lower than that of configuration D. However, the modal loss factor for these modes is significantly higher for configuration C. The same applies to the second bending mode at 20°C (b). Although the material loss factor is higher for configuration C, the damping performance of configuration D is superior.

From these observations, it can be concluded that the changes in storage modulus have a greater impact on the vibration damping than the material loss factor. In fact, a higher material loss factor will not compensate for an inappropriate design.

As a consequence, it is not sufficient to tune only the eigenfrequencies of a vibrating CLD system with respect to the glass transition region of a viscoelastic material. Instead, more effort must be invested to establish an appropriate shear stiffness of the additional CLD layers. This objective is difficult to accomplish when the operating temperatures are far apart from each other. In the considered case, it is advantageous to design wide layers at antinodes and slim layers at nodes or free ends for low temperature. The opposite applies for high temperatures.

However, it is important to emphasize that the optimal design is sensitive to other system and structural parameters, such as layer thicknesses or boundary conditions. Any modification will affect the resulting structural behavior and requires a detailed analysis of the optimal design. As a consequence, a general, temperature-dependent design guideline cannot be derived.

5.3. *Experimental validation*

In order to validate the numerical results obtained in the previous sections, an experiment was performed under laboratory conditions. In this context, the optimal design configuration 1D (see Table 7) was selected for validation and the corresponding parts of the host structure, core and face layers were manufactured accordingly. The metallic layers are made of aluminum with thicknesses and material properties as shown in Table 1. The elastomer layer was cut out from a vulcanized bromobutyl rubber mat. Since rolling of the elastomer compound prior to vulcanization is not a high-precision manufacturing technique, the thickness of the elastomeric strip is slightly inhomogeneous, varying from 1.85 mm at one end to 2 mm at the other end. After assembling the sandwich by conglutinating the layers with Loctite 480, the total thickness of the CLD beam differs between 15.08 mm and 15.18 mm. This means that the adhesive contributes about 0.2 mm to the total thickness of the CLD laminate. While the influence of the adhesive is neglected, the thickness of the viscoelastic layer is assumed to be constant and is set to 1.9 mm in the numerical simulation.

Fig. 14 shows the modal test setup. The measurement is performed at an ambient temperature of 20°C. The composite beam is suspended at one end and two acceleration sensors are attached to the other end. Similar tests have been performed on previous samples using a scanning laser-vibrometer. Therefore, the mode shapes and their sequence are generally known. Bending and torsion modes occur in the considered frequency bandwidth between 0 and 1500 Hz. Consequently, at least two response sensors are required to distinguish between bending and torsion modes. The structure is excited by an automated modal hammer and the force and acceleration time data are acquired. The driving point is chosen to be the back side of the position of sensor 1. In a next step, the time data are processed by a rectangular window for the force channel and an exponential window for the response channels. A Fast Fourier Transformation is applied and the corresponding power spectral densities are determined. The frequency response functions (FRFs) are calculated and averaged for multiple impacts (10 in total). Finally, the PolyMAX algorithm of the Siemens Testlab software is used to identify the eigenfrequencies, modal damping ratios and mode shapes from the FRFs. The PolyMAX algorithm is a multi-degree-of-freedom frequency domain identification method that is based on the least-squares principle and explained in [52]. The common procedure and the mathematical methods for signal processing and experimental modal analysis are well documented in [53].

Fig. 15 shows a Bode plot of the host structure (undamped beam) compared to the CLD configuration. It is evident that the additional CLD layers significantly attenuate the resonance peaks. The damping effect can also be seen in the wider resonance peaks and flatter slopes of the phase response when passing through a resonance. Due to the changes in mass and stiffness, the sequence of the third bending (3. BM) and torsion (1. TM) modes has changed compared to the undamped beam. Furthermore, tiny peaks appear that correspond to the transverse bending modes. These modes are barely visible because the structure is weakly excited in the transverse direction and the sensor measured little response due to the transverse sensitivity (i.e. crosstalk) of the acceleration sensors used.

The comparison of eigenfrequencies and damping ratios between simulation and experimental data can be found in Table 8. It is remarkable that the eigenfrequencies correlate with considerable accuracy ($\Delta f < 1$ %). In opposite, the simulated damping ratios deviate slightly from the identified damping. The simulated damping is always underestimated. The deviation of the damping has several reasons. On the one hand, the damping ratio is known to be a very sensitive parameter in modal identification and strongly depends on the evaluation bandwidth and the excitation level of a mode shape (i.e. modal participation). On the other hand, the PolyMAX algorithm fits the synthetic FRF based on the linear viscous damping model. As a consequence, the frequency dependence of the viscoelastic material damping is not considered, leading to an erroneous identification that reflects the best possible viscous damping fit to a structure with frequency-dependent hysteretic damping. However, the state of the art does not provide a feasible identification method for viscoelastic damping. In addition, similar damping and even larger deviations are reported by Kim et al. [37] and Leibowitz and Lifshitz [54]. Under these circumstances, a damping deviation of 6.93 % and less is acceptable and the numerical prediction is considered valid.

The experimental validation has proven that the simulated system behavior can be reproduced in reality. Considering that the simulation is based on a rather complex, frequency- and temperature-dependent viscoelastic material model, it is also remarkable that the modal parameters resulting from both numerical and experimental analysis are in good agreement.

6. Conclusion

A novel approach for shape optimization of CLD beams was presented and applied to viscoelastic damping maximization in an FE environment. Considering a mass constraint, a modified Gauss-Seidel method was employed to sequentially determine multiple widths of the viscoelastic core and the elastic face layer. A comparison of the modal loss factors with those obtained from other placement strategies demonstrated the efficiency of the proposed approach. Additionally, the influence of storage modulus and ambient temperature on the optimal damping design for the first three bending modes was examined. The results evidenced the temperature-sensitivity, which led to opposite optimal CLD designs for the considered temperatures. Finally, a modal impact test was performed to experimentally validate the expected damping of an optimal CLD design at room temperature.

The following conclusions can be drawn from the results of the present study:

I. The most important finding is that the width of the core and face layer is a feasible design parameter for damping optimization of CLD beams.
II. An additional damping improvement can be achieved by dividing the width into several sections along the longitudinal axis of a beam-like structure. At the same time, summarizing individual element sections as design variables and the use of symmetry properties of considered mode shapes, reduce the numerical effort of the presented optimization approach.
III. The optimal design of a CLD treatment is temperature-dependent, whereas the temperature sensitivity is mostly driven by changes in the storage modulus and not by changes in the loss factor of the viscoelastic material. Therefore, it is not recommended to design a CLD treatment with the sole objective of shifting a particular eigenfrequency towards the glass transition region of the viscoelastic material.
IV. The design of a CLD treatment is optimal only for the considered design temperature and can be less efficient at off-design temperatures.
V. A generalized guideline for optimal CLD design cannot be derived. Rather, since the damping performance of CLD treatments depends significantly on the mode shape as well as on the geometrical, material and environmental properties, each CLD treatment should be individually designed to achieve the most efficient damping performance.

The present study lays the foundation for future work. Possible improvements of the present approach encompass the inclusion of additional design parameters such as the layer thicknesses of the core and face layers and the adaptation to plate-like structures. Experimental analyses will be performed in the low temperature region to further verify the temperature dependence of optimal CLD designs.

CRediT authorship contribution statement

Martin Gröhlich: Conceptualization, Methodology, Software, Validation, Formal analysis, Writing – original draft. **Marc Böswald:** Conceptualization, Writing – review & editing, Supervision. **Jörg Wallaschek:** Conceptualization, Writing – review & editing, Supervision.

Declaration of Competing Interest

The authors declare that they have no known competing financial interests or personal relationships that could have appeared to influence the work reported in this paper.

Data availability

Data will be made available on request.

Table A.1
Model parameters of the Generalized Maxwell-Model of the elastomer compound. Here, the letter e corresponds to an exponential basis of 10, so that e.g. 3.162e+03 is equal to $3.162 \cdot 10^3$.

	Index i						
Parameter	1	2	3	4	5	6	7
τ_i (s)	1.000e+04	3.162e+03	1.000e+03	3.162e+02	1.000e+02	3.162e+01	1.000e+01
G_i (Pa)	4.045e+04	4.276e+04	5.985e+04	7.428e+04	5.995e+04	7.379e+04	7.967e+04
	8	9	10	11	12	13	14
τ_i (s)	3.162e+00	1.000e+00	3.162e-01	1.000e-01	3.162e-02	1.000e-02	3.162e-03
G_i (Pa)	8.387e+04	1.049e+05	1.250e+05	1.614e+05	2.278e+05	3.341e+05	5.495e+05
	15	16	17	18	19	20	21
τ_i (s)	1.000e-03	3.162e-04	1.000e-04	3.162e-05	1.000e-05	3.162e-06	1.000e-06
G_i (Pa)	1.002e+06	1.962e+06	3.824e+06	7.580e+06	1.526e+07	2.651e+07	4.224e+07
	22	23	24	25	26	27	inf
τ_i (s)	3.162e-07	1.000e-07	3.162e-08	1.000e-08	3.162e-09	1.000e-09	-
G_i (Pa)	5.911e+07	6.895e+07	9.909e+07	1.610e+08	1.164e+02	2.538e-01	7.473e+05

Table A.2
WLF and Arrhenius parameters of the elastomer compound for horizontal and vertical shifting.

C_1 (-)	C_2 (K)	T_{ref} (K)	$b_{T,E'}$ (J/mol)	$b_{T,E'}$ (J/mol)
7.26	166.25	293.15	2010	2010

Acknowledgements

We would like to acknowledge the funding by the Deutsche Forschungsgemeinschaft (DFG, German Research Foundation) under Germany's Excellence Strategy – EXC 2163/1- Sustainable and Energy Efficient Aviation – Project-ID 390881007.

Furthermore, we would like to acknowledge the support of our colleague Tobias Meier who was taking over the manufacturing of the core and face layer and the assembly with the host structure.

Appendix A. Model parameters of the elastomer compound

References

[1] M.D. Rao, Recent applications of viscoelastic damping for noise control in automobiles and commercial airplanes, J. Sound Vib. 262 (3) (2003) 457–474.
[2] A.D. Nashif, D.I. Jones, J.P. Henderson, Vibration Damping, Wiley, New York, 1985.
[3] A.R. Payne, The dynamic properties of carbon black-loaded natural rubber vulcanizates. Part I, J. Appl. Polym. Sci. 6 (19) (1962) 57–63.
[4] A.R. Payne, The dynamic properties of carbon black-loaded natural rubber vulcanizates. Part II, J. Appl. Polym. Sci. 6 (21) (1962) 368–372.
[5] M.L. Williams, R.F. Landel, J.D. Ferry, The temperature dependence of relaxation mechanisms in amorphous polymers and other glass-forming liquids, J. Am. Chem. Soc. 77 (14) (1955) 3701–3707.
[6] R.M. Christensen, Theory of viscoelasticity: An introduction, Academic Press Inc., New York, 1982.
[7] H.F. Brinson, L.C. Brinson, Polymer Engineering Science and Viscoelasticity, Springer, New York, 2008.
[8] B.C. Chakraborty, D. Ratna, Polymers For Vibration Damping Applications, Elsevier, Amsterdam, 2020.
[9] D.J. McTavish, P.C. Hughes, Modeling of linear viscoelastic space structures, J. Vib. Acoust. 115 (1) (1993) 103–110.
[10] R.L. Bagley, P.J. Torvik, Fractional calculus - a different approach to the analysis of viscoelastically damped structures, AIAA J. 21 (5) (1983) 741–748.
[11] G.A. Lesieutre, E. Bianchini, Time domain modeling of linear viscoelasticity using anelastic displacement Fields, J. Vib. Acoust. 117 (4) (1995) 424–430.
[12] C.M.A. Vasques, R.A.S. Moreira, J.D. Rodrigues, Viscoelastic damping technologies - Part I: modeling and finite element implementation, J. Adv. Res. Mech. Eng. 1 (2) (2010) 76–95.
[13] X.Q. Zhou, D.Y. Yu, X.Y. Shao, S.Q. Zhang, S. Wang, Research and applications of viscoelastic vibration damping materials: a review, Comp. Struct. 136 (2016) 460–480.
[14] E.M. Kerwin, Damping of flexural waves by a constrained viscoelastic layer, J. Acoust. Soc. Am. 31 (7) (1959) 952–962.
[15] D. Ross, E.E. Ungar, E.M. Kerwin, Damping of plate flexural vibrations by means of viscoelastic laminae, Struct. Damp. (1959) 49–87.
[16] R.A. Di Taranto, Theory of vibratory bending for elastic and viscoelastic layered finite-length beams, ASME J. Appl. Mech. 32 (4) (1965) 881–886.
[17] D.J. Mead, S. Markus, The forced vibration of a three-layer, damped sandwich beam with arbitrary boundary conditions, J. Sound Vib. 10 (2) (1969) 163–175.
[18] D.K. Rao, Frequency and loss factors of sandwich beams under various boundary conditions, J. Mech. Eng. Sci. 20 (5) (1978) 271–282.
[19] R.A.S. Moreira, J.D. Rodrigues, Constrained damping layer treatments: finite element modeling, J. Vib. Control 10 (4) (2004) 575–595.
[20] R.A.S. Moreira, J.D. Rodrigues, A layerwise model for thin soft core sandwich plates, Comp. Struct. 84 (19) (2006) 1256–1263.
[21] R.A.S. Moreira, J.D. Rodrigues, A.J.M. Ferreira, A generalized layerwise finite element for multi-layer damping treatments, Comput. Mech. 37 (5) (2006) 426–444.
[22] A.L. Araújo, C.M.M. Soares, C.A.M. Soares, A viscoelastic sandwich finite element model for the analysis of passive, active and hybrid structures, Appl. Compos. Mater. 17 (5) (2010) 529–542.

[23] A.L. Araújo, C.M.M. Soares, C.A.M. Soares, Finite element model for hybrid active-passive damping analysis of anisotropic laminated sandwich structures, J. Sandw. Struct. Mater. 12 (4) (2010) 397–419.
[24] H. Li, Z. Wang, H. Lv, Z. Zhou, Q. Han, J. Liu, Z. Qin, Nonlinear vibration analysis of fiber reinforced composite cylindrical shells with partial constrained layer damping treatment, Thin Wall. Struct. 157 (2020), 107000.
[25] H. Li, Z. Li, B. Safaei, W. Rong, W. Wang, Z. Qin, J. Xiong, Nonlinear vibration analysis of fiber metal laminated plates with multiple viscoelastic layers, Thin Wall Struct. 168 (2021), 108297.
[26] H. Li, W. Wang, Q. Wang, Q. Han, J. Liu, Z. Qin, J. Xiong, X. Wang, Static and dynamic performances of sandwich plates with magnetorheological elastomer core: theoretical and experimental studies, J. Sandw. Struct. Mater. 24 (3) (2022) 1556–1579.
[27] H. Li, X. Wang, J. Sun, S.K. Ha, Z. Guan, Theoretical and experimental investigations on active vibration control of the MRE multifunctional grille composite sandwich plates, Comp. Struct. 295 (2022), 115783.
[28] J.M. Lifshitz, M. Leibowitz, Optimal sandwich beam design for maximum viscoelastic damping, Int. J. Solids Struct. 23 (7) (1987) 1027–1034.
[29] J.-.L. Marcelin, P. Trompette, A. Smati, Optimal constrained layer damping with partial coverage, Finite Elem. Anal. Des. 12 (3) (1992) 273–280.
[30] J.-.L. Marcelin, S. Shakhesi, F. Pourroy, Optimal constrained layer damping of beams: experimental and numerical studies, Shock Vib. 2 (6) (1995) 445–450.
[31] M. Alvelid, Optimal position and shape of applied damping material, J. Sound Vib. 310 (4) (2008) 947–965.
[32] G. Lepoittevin, G. Kress, Optimization of segmented constrained layer damping with mathematical programming using strain energy analysis and modal data, Mater. Des. 31 (1) (2010) 14–24.
[33] A.L. Araújo, P. Martins, C.M.M. Soares, C.A.M. Soares, J. Herskovits, Damping optimization of viscoelastic laminated sandwich composite structures, Struct. Multidiscip. Optim. 39 (6) (2009) 569–579.
[34] J.F.A. Madeira, A.L. Araújo, C.M.M. Soares, C.A.M. Soares, A.J.M. Ferreira, Multiobjective design of viscoelastic laminated composite sandwich panels, Compos. Part B-Eng. 77 (2015) 391–401.
[35] M.P. Bendsøe, O. Sigmund, Topology Optimization: Theory, Methods and Applications, Springer, Berlin, 2004.
[36] Z. Ling, X. Ronglu, W. Yi, A. El-Sabbagh, Topology optimization of constrained layer damping on plates using Method of Moving Asymptote (MMA) approach, Shock Vib 18 (1–2) (2011) 221–244.
[37] S.Y. Kim, C.K. Mechefske, I.Y. Kim, Optimal damping layout in a shell structure using topology optimization, J. Sound Vib. 332 (12) (2013) 2873–2883.
[38] W. Zheng, Y. Lei, S. Li, Q. Huang, Topology optimization of passive constrained layer damping with partial coverage on plate, Shock Vib. 20 (2) (2013) 199–211.
[39] Z. Fang, L. Zheng, Topology optimization for minimizing the resonant response of plates with constrained layer damping treatment, Shock Vib. 2015 (2015), 376854.
[40] D. Zhang, T. Qi, L. Zheng, A hierarchical optimization strategy for position and thickness optimization of constrained layer damping/plate to minimize sound radiation power, Adv. Mech. Eng. 10 (10) (2018) 1–15.
[41] E.R. Fotsing, M. Sola, A. Ross, E. Ruiz, Lightweight damping of composite sandwich beams: experimental analysis, J. Comp. Mater. 47 (12) (2013) 1501–1511.
[42] N. Kumar, S.P. Singh, Experimental study on vibration and damping of curved panel treated with constrained viscoelastic layer, Compos. Struct. 92 (2) (2010) 233–243.
[43] N. Kumar, S.P. Singh, Vibration control of curved panel using smart damping, Mech. Sys. Signal Pr. 30 (2012) 232–247.
[44] M. Gröhlich, M. Böswald, R. Winter, Finite element optimization of viscoelastic damping applications, in: Proceedings of ISMA 2020 International Conferenceon Noise and Vibration Engineering, Leuven, 2020.
[45] J. Fritzsche, M. Klüppel, Structural dynamics and interfacial properties of filler-reinforced elastomers, J. Phys.-Condens. Mat. 23 (3) (2011), 035104.
[46] M. Gröhlich, A. Lang, M. Böswald, J. Meier, Viscoelastic damping design - Thermal impact on a constrained layer damping treatment, Mater. Des. 207 (2021), 109885.
[47] L. Rouleau, J.-.F. Deü, A. Legay, A comparison of model reduction techniques based on modal projection for structures with frequency-dependent damping, Mech. Sys. Signal Pr. 90 (2017) 110–125.
[48] M. Gröhlich, M. Böswald, R. Winter, An iterative eigenvalue solver for systems with frequency dependent material properties, in: Proceedings of the DAGA 2020, Hannover, 2020.
[49] R.J. Allemang, The modal assurance criterion - twenty years of use and abuse, Sound Vib. 37 (8) (2003) 14–23.
[50] M. Gröhlich, M. Böswald, R. Winter, Frequency and temperature dependent viscoelastic vibration damping capability of a novel local CLD treatment, in: Proceeding of INTER-NOISE 2019, Madrid, 2019.
[51] M. Gröhlich, M. Böswald, R. Winter, Vibration damping capabilities of treatments with frequency and temperature dependent viscoelastic material properties, in: Proceedings of ICA 2019 - 23rd International Congress on Acoustics, Aachen, 2019.
[52] B. Peeters, H.V. der Auweraer, P. Guillaume, J. Leuridan, The PolyMAX frequency-domain method: a new standard for modal parameter estimation? Shock Vib. 11 (2004) 395–409.
[53] D.J. Ewins, Modal Testing: theory, Practice and Application, Research Studies Press Ltd., Hertfordshire, 2000.
[54] M. Leibowitz, J.M. Lifshitz, Experimental verification of modal parameters for 3-layered sandwich beams, Int. J. Solids Struct. 26 (2) (1990) 175–184.